



Contents lists available at ScienceDirect

Arabian Journal of Chemistry

journal homepage: www.ksu.edu.sa

Towards a better understanding on adsorption mechanism of various heavy metal with phosphorus rich hydrochar

Yi Wen, Dingxiang Chen, Yong Zhang, Huabin Wang*, Rui Xu*

School of Energy and Environment Science, Yunnan Normal University, Kunming 650500, PR China
Yunnan Key Laboratory of Rural Energy Engineering, Kunming 650500, PR China

ARTICLE INFO

Keywords:

Adsorption mechanism
Heavy metal
Phosphorus
Hydrochar
Cow manure

ABSTRACT

The heavy metal contents in many rivers and groundwater exceeds safety standards, and hydrochar stands out among many functional materials for environmental protection applications as its efficient and low-cost. The influence of endogenous phosphorus in the adsorption and the forms of heavy metal combined with phosphorus are not always fully explored. Thus, the purpose of this study was to clarify adsorption mechanism as well as the biological risks. The physisorption and chemisorption likely coexisted during adsorption of Pb(II) and Hg(II), while physisorption dominated Cd(II) adsorption. The adsorption isotherms of three heavy metal were well fitted with the Langmuir model with capacity of 466.45, 339.48, and 264.19 mg·g⁻¹, respectively. The ion-exchange was the dominant mechanism for Pb(II) and Cd(II) adsorptions. The precipitations were mainly phosphate and carbonate, respectively. On the contrary, formation of complexations was considered as the dominant mechanism for Hg(II) adsorption. Thus, the contribution of phosphorus in adsorption was: Pb(II) > Cd(II) > Hg(II). Using CMHCC to remove heavy metal not only had great effect, but also little harm of eutrophication caused by endogenous phosphorus release for the proportion of bioavailable phosphorus decreased. It's worth noting that the biological risk of CMHCC@HM was: CMHCC@Pb > CMHCC@Cd > CMHCC@Hg. The present study explored the role of endogenous phosphorus in the adsorption of different heavy metal, and the forms of heavy metal and phosphorus. The study improved the effect of hydrochar endogenous substances on heavy metal adsorption.

1. Introduction

With the rapid population growth and accelerated industrialization, heavy metal pollution is becoming increasingly serious, with the heavy metal content in many rivers and groundwater exceeds safety standards (Kumar et al., 2022). The Pb(II), Cd(II), and Hg(II) remediation was discussed due to their high toxicity and high occurrence as a pollutant, especially from industrial waste, when compared to other metals (Bao et al., 2022).

The effective treatment methods for removing heavy metal from polluted water mainly include chemical precipitation, electrochemical redox, ion-exchange, adsorption and membrane separation (Qiu et al., 2021). In contrast, the adsorption method has the advantages of simple operation, high removal rate and low cost (Wang et al., 2023a). As an efficient and low-cost adsorbent, biochar stands out among many new functional materials for environmental protection applications, and has attracted extensive attention and research in the field of heavy metal

polluted water treatment (Kumar et al., 2021). At present, the use of biochar as an adsorbent to adsorb and remove metals has become a common method. Hydrothermal processing of biomass may be able to overcome a series of problems associated with the thermochemical conversion of lignocellulosic material into energy and fuels (Teribele et al., 2023).

Due to the various biomass materials, the elemental composition of biochar is different. When biochar is applied, the endogenous substances will be released into solution. These released endogenous substances may promote the adsorption effect of biochar. The alkali metal ions (K⁺, Ca²⁺, Na⁺, Mg²⁺, etc.) contained in biochar can exchange heavy metal ions, moreover, the soluble anions (CO₃²⁻, SO₄²⁻, PO₄³⁻, etc.) released can be precipitated with heavy metal ions (Yang et al., 2023).

Generally, phosphorus-rich biochar consists of the following categories: sludge, phosphorus-modified biochar, phosphorus-rich plant, and manure sources of biochar. Manure production has increased dramatically each year as a result of the recent rapid expansion of

Peer review under responsibility of King Saud University. Production and hosting by Elsevier.

* Corresponding authors.

E-mail addresses: hbwang@ynnu.edu.cn (H. Wang), ecowatch_xr@163.com (R. Xu).<https://doi.org/10.1016/j.arabjc.2023.105530>

Received 20 July 2023; Accepted 4 December 2023

Available online 6 December 2023

1878-5352/© 2023 The Author(s). Published by Elsevier B.V. on behalf of King Saud University. This is an open access article under the CC BY-NC-ND license (<http://creativecommons.org/licenses/by-nc-nd/4.0/>).

concentrated animal feeding operations in many parts of the world. The accumulation of cow manure on farms cause a negative impact on the environment (Szogi et al., 2020), for a 1000 lb cow will produce 60 lb of manure per day. Therefore, it is imperative to find solutions for the processing and usage of cow manure. The previous research found that cow manure biochar released of phosphorus when it was placed in solution with the phosphorus content up to $0.33\text{--}0.62\text{ mg}\cdot\text{g}^{-1}$ (Wang et al., 2023b). In addition to phosphate modification, biochar prepared with phosphorus – rich waste also had a good adsorption effect. The banana peel biochar modified by K_3PO_4 showed a great adsorption effect of Pb (II) (Ge et al., 2022), and the adsorption capacity of kitchen waste biochar modified by K_2HPO_4 reached $257.95\text{ mg}\cdot\text{g}^{-1}$ (Ning et al., 2022). The adsorption capacity of swine manure biochar reached $287.87\text{ mg}\cdot\text{g}^{-1}$ (Sun et al., 2022). Phosphate – modified biochar had a good adsorption effect, but researchers on phosphate – modified biochar were prone to ignore the role of endogenous phosphorus of the material for heavy metal adsorption. That is to say, the contribution of endogenous phosphorus in adsorption is ill – defined. Therefore, this research intended to explore the contribution of adsorption mechanism of phosphorus – loaded hydrochar, so as to explore the contribution of phosphorus.

The release of endogenous phosphorus is not only closely related to the adsorption effect of heavy metal, but also may result in eutrophication. Biochar containing phosphorus is applied to river and soil. Although biochar solidifies heavy metal, the forms of heavy metal and phosphorus affect the environmental risk. Researchers have been working on the magnetical biochar, but it still is difficult to separate and recover biochar applied to soil. Moreover, the role of inherent P in biochar in affecting soil P cycle received little attention (Chen et al., 2022). Therefore, it is necessary to study the forms of heavy metal and phosphorus to assess environmental risks caused by biochar.

To sum up, the role and influence of endogenous phosphorus in the adsorption process of different heavy metal, as well as the forms of heavy metal and phosphorus are not always fully explored. Thus, the purpose of this study was to clarify the reason for the change of phosphorus content during the adsorption of three heavy metal by cow manure hydrothermal carbonization carbon (CMHCC), and the adsorption mechanism of three heavy metal. By XRD, FTIR and XPS analysis, the possible adsorption mechanism was explored, and by calculation, the ratio of different adsorption mechanisms of Pb(II), Cd(II), and Hg(II) was investigated. This study improved the effect of hydrochar

endogenous substances on heavy metal adsorption.

2. Materials and methods

2.1. Experimental material

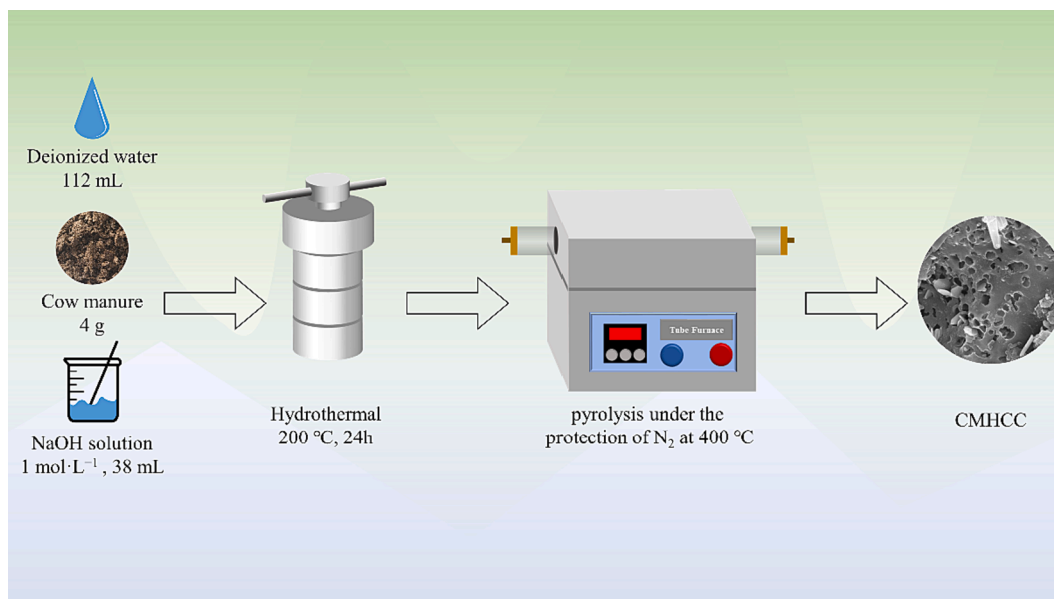
The cow manure was collected from the Laohadu Demonstration Ranch in Mengzi City, Yunnan Province, China. The CM were oven-dried at $85\text{ }^\circ\text{C}$ for 24 h, and sieved through 100–meshes. The primary chemical, e.g. $\text{Pb}(\text{NO}_3)_2\cdot 3\text{H}_2\text{O}$, $\text{Cd}(\text{NO}_3)_2\cdot 4\text{H}_2\text{O}$, and HgCl_2 , superior grade HNO_3 (65 – 68 %), and the analytically pure chemical, e.g. NaOH and HCl used in this study were purchased from Beijing Chemical Reagent Factory.

2.2. Production of CMHCC

The preparation method followed the previous work of the group (Wang et al., 2023b), and the preparation process is shown in Scheme 1. Briefly, fresh cow manure was dried at $85\text{ }^\circ\text{C}$ and ground (100 – mesh). Firstly, 4 g dried CM, 112 mL deionized water, and 38 mL of NaOH solution ($1\text{ mol}\cdot\text{L}^{-1}$) were mixed. Secondly, the mixture was shaken with ultrasound for 30 min and stirred for another 2 h. Thirdly, the mixture was hydrothermally heated at $200\text{ }^\circ\text{C}$ for 24 h and then rinsed with acetone. Finally, the mixture was dried at $85\text{ }^\circ\text{C}$. CMBC was obtained via pyrolysis under the protection of N_2 at $400\text{ }^\circ\text{C}$ for 1 h, denoted as CMHCC.

2.3. Analysis methods

The elemental composition (EA) of CMHCC was analyzed with elemental analyzer (Elementar Vario EL cube, Germany). The Scanning Electron Microscope (SEM) instrument was applied for the microstructure analysis of CMHCC and three kinds of hydrochar after adsorbing Pb (II), Cd(II), and Hg(II) in the same conditions at 5 kV (Mira LMS, Tescan, Czech Republic). The specific surface area (SSA) of hydrochar was detected by N_2 adsorption isotherms at 77 K using a Micropore Analyzer (ASAP 2460, Micromeritics, United States). The electron binding energy and elemental valence were analyzed using X – ray photoelectron spectroscopy (XPS) (K–Alpha, Thermo Scientific, United States). The functional groups were qualitatively examined using a Fourier transform infrared spectrometer (FTIR) (Niolet iN10EA, Thermo Scientific, United



Scheme 1. The preparation process of CMHCC.

States). The amount of the elements in the solutions was determined by inductively coupled plasma mass spectrometry (ICP) (Thermo Fisher–X series, United States).

3. Experimental designs

3.1. Endogenous phosphorus leaching experiments

The 20 mg of CMHCC was weighed, then the 20 mL deionized water (pH = 2, 4, and 6) was added. After oscillation (200 rpm·min⁻¹, 25 °C), 5 mL solution was filtered (0.22 μm) at predetermined times (0.5, 1, 2, 4, 6, 12, 18, and 24 h), and the phosphorus contents were determined via ICP. And the HCl and NaOH solutions were used to adjust the pH of deionized water.

3.2. Adsorption experiments

3.2.1. Adsorption kinetics

There were three different types of heavy metal with divalent used to investigate the adsorption effect of CMHCC: Pb(II), Cd(II), and Hg(II). A mixture of 20 mg CMHCC and 20 mL of 100 mg·L⁻¹ Pb(NO₃)₂, Cd(NO₃)₂, or HgCl₂ solution was added to a 25 mL glass bottle at room temperature (25 °C), and the initial pH of the mixture was adjusted to 6.0 by HNO₃ or NaOH solutions. Concentration of the adsorbent was maintained at 1 g·L⁻¹ in all the treatments. The glass bottles containing CMHCC and heavy metal solution were shaken in a thermostatic reciprocating shaker at 200 rpm·min⁻¹. After oscillation (200 rpm·min⁻¹, 25 °C), 5 mL solution was filtered (0.22 μm) at predetermined times (0.5, 1, 2, 4, 6, 12, 18, and 24 h), and the filtrate obtained from each bottle by immediate filtration of the suspension through a nylon membrane filter with a pore size of 0.22 μm was stored at 4 °C. The contents of phosphorus and heavy metal were determined via ICP. The adsorption capacities of Pb(II), Cd(II), and Hg(II) were calculated using Eq. (1) and the experimental results were fitted using the adsorption dynamic model (Eqs. (2) and (3)).

$$Q_e = (C_0 - C_e) \times \frac{V_0}{m} \quad (1)$$

$$Q_t = Q_e (1 - e^{-k_1 t}) \quad (2)$$

$$\frac{t}{Q_t} = \frac{1}{k_2 Q_e^2} + \frac{t}{Q_e} \quad (3)$$

In the equations, Q_e represented the equilibrium adsorption capacity in mg·g⁻¹; C_0 and C_e represent the mass concentration of Pb(II), Cd(II) or Hg(II) at the initial and adsorption equilibrium in mg·g⁻¹, respectively; V_0 was the volume of the heavy metal solution in L; and m represented the dosage of hydrochar in g; Q_t represented the adsorption capacity at time t in mg·L⁻¹; k_1 represented the reaction rate constant of the pseudo – first – order model in min⁻¹; k_2 was the reaction rate constant of the pseudo – second – order model in g·(mg·min)⁻¹; and a and b were the initial adsorption rate and activation energy – related constants in mg·(g·min)⁻¹ and g·mg⁻¹, respectively.

3.2.2. Adsorption isotherms

The adsorption isotherm experiments were carried out to determine the adsorption capacity of CMHCC for Pb(II), Cd(II), and Hg(II). 20 mg of CMHCC was weighed and mixed with 20 mL of three kinds of heavy metal solution containing various concentrations (100, 200, 300, 400, 500, and 600 mg·L⁻¹) in a 25 mL glass bottle and the initial pH of the mixture was adjusted to 6.0 by HNO₃ or NaOH solutions. After 24 h of oscillation (200 rpm·min⁻¹, 25 °C), the filtrate from each glass bottle was collected after filtering the suspension and was stored at 4 °C. The contents of phosphorus and heavy metal were determined via ICP, respectively. The adsorption capacities of Pb(II), Cd(II), and Hg(II) were calculated using Eq. (1), and the experimental results were fitted using

and the isothermal adsorption model (Eqs. (4) and (5)).

$$Q_e = \frac{Q_m C_e K_L}{1 + K_L C_e} \quad (4)$$

$$Q_e = K_F C_e^n \quad (5)$$

In the equations, Q_e represented the equilibrium adsorption capacity in mg·g⁻¹; C_0 and C_e represent the mass concentration of Pb(II), Cd(II) or Hg(II) at the initial and adsorption equilibrium in mg·g⁻¹, respectively; Q_m represented the theoretical maximum adsorption capacity in mg·g⁻¹; K_L represented the equilibrium constant of the Langmuir model; K_F was the Freundlich constant, and n was the empirical constant.

3.2.3. Effect of initial pH on adsorption

The initial solution pH value affects the degree of protonation of functional groups on the adsorbent surface. It also changes the existing forms of heavy metal ions in solution [31]. At low pH values (pH less than 3), the protonation of surface functional groups made the surface of CMHCC positively charged, which had a repulsion effect on heavy metal cations. In addition, a large number of H₃O⁺ competed with Pb(II), Cd(II), and Hg(II) to occupy the adsorption site (Su et al., 2022).

A mixture of 20 mg CMHCC and 20 mL of 100 mg·L⁻¹ Pb(NO₃)₂, Cd(NO₃)₂, or HgCl₂ solution was added to a 25 mL glass bottle at room temperature (25 °C). The initial pH of the mixture was adjusted to a fixed value within the range of 2 – 6 using HNO₃ or NaOH solution, and the mixtures were shaken in a thermostatic reciprocating shaker at 200 r·min⁻¹ for 24 h at room temperature (25 °C). At the end of shaking, final pH was measured again, and the contents of phosphorus and heavy metal were determined via ICP. The effect of pH on the adsorption by CMHCC was studied in solution varying pH from 2 to 6, because the gray precipitate would be produced in HgCl₂ solution when pH ≥ 7.

3.3. Extraction method of phosphorus

The three kinds of hydrochar after adsorbing Pb(II), Cd(II), and Hg(II) were marked as CMHCC@Pb, CMHCC@Cd, and CMHCC@Hg, respectively. In addition, these three hydrochar were collectively called CMHCC@HM. The morphology of inorganic phosphorus in CMHCC@Pb, CMHCC@Cd, CMHCC@Hg, and CMHCC was determined by four – step continuous extraction method (Jun et al., 2005, Li et al., 2023) This extraction method was proposed on the basis of method of Hieltjes – Lijklema and method of Ruttenberg (Hieltjes and Lijklema, 1980, Long et al., 2023).

Firstly, 20 mg CMHCC@Pb, CMHCC@Cd, CMHCC@Hg, and CMHCC was added into 50 mL centrifuge tubes respectively, and 20 mL NH₄Cl solution (1 mol·L⁻¹) was added. After shaken for 30 min at 25 °C, the centrifuge tubes were centrifuged (5000 rpm·min⁻¹, 10 min) to achieve solid – liquid separation. The filtrate obtained from each centrifuge tube through a nylon membrane filter with a pore size of 0.22 μm was stored at 4 °C. Secondly, 20 mL NaHCO₃ – Na₂S₂O₃ solution (0.11 mol·L⁻¹) was added into the centrifuge tube with residue solids. After shaken for 60 min at 25 °C, the centrifuge tubes were centrifuged (5000 rpm·min⁻¹, 10 min) and the filtrate obtained from each centrifuge tube through a nylon membrane filter with a pore size of 0.22 μm was stored at 4 °C. Thirdly, 20 mL NaOH solution (1 mol·L⁻¹) was added into the centrifuge tube with residue solids. After shaken for 16 h at 25 °C, repeated the centrifugation and filtration. Fourthly, 20 mL HCl solution (0.5 mol·L⁻¹) was added into the centrifuge tube with residue solids. After shaken for 16 h at 25 °C, repeated the centrifugation and filtration. The phosphorus content of filtrate obtained at each step was determined via ICP, and denoted as L – P, RSP, Fe/Al – P, and Ca – P, sequentially.

3.4. Sequential extraction method of heavy metal

After CMHCC adsorbed three kinds of heavy metal, CMHCC@HM were collected for measurement by a simplified sequential extraction

method (Liu et al., 2023). Herein, the heavy metal immobilized on CMHCC@HM were classified into three parts, including exchangeable, acid soluble and generally stable heavy metal.

Firstly, dried residual solids and 0.5 mol MgCl_2 (adjust to $\text{pH} = 7$ using NaOH or HCl) were mixed at a ratio of $1/80$ ($\text{mg}\cdot\text{L}^{-1}$) and shaken for 20 min at 25°C . Secondly, another dried residual solids and 1 mol NaOAc (adjust to $\text{pH} 5.0$ with NaOH or HOAc) at the same ratio, subsequently shaken for 5 h at 25°C . Finally, the extracted solution was filtered with $0.22\ \mu\text{m}$ filter membrane and determined via ICP. The calculation method of the concentration of three parts was shown as Equations (6) – (11).

$$HM_{ex,M} = C_{1,M} \times V/w \quad (6)$$

$$HM_{ac,M} = (C_{2,M} - C_{1,M})V/w \quad (7)$$

$$HM_{ge,M} = HM_{tot,M} - HM_{ex,M} - HM_{ac,M} \quad (8)$$

$$W_{ex,M} = HM_{ex,M}/HM_{tot,M} \quad (9)$$

$$W_{ac,M} = HM_{ac,M}/HM_{tot,M} \quad (10)$$

$$W_{ge,M} = HM_{ge,M}/HM_{tot,M} \quad (11)$$

In the above formula, $C_{1,M}$ ($\text{mg}\cdot\text{L}^{-1}$) represented the concentration of heavy metal ions (mol) extracted from the first step. $C_{2,M}$ ($\text{mg}\cdot\text{L}^{-1}$) represented the concentration of heavy metal ions extracted from the second step. w and V represented the mass of adsorbent and the volume of extraction solution. $HM_{ex,M}$ and $W_{ex,M}$ represented the content and proportion of exchangeable state of heavy metal on CMHCC, respectively. $HM_{ac,M}$ and $W_{ac,M}$ represented the content and proportion of acid soluble state of heavy metal on CMHCC, respectively. $HM_{ge,M}$ and $W_{ge,M}$ represented the content and proportion of generally stable state of heavy metal on CMHCC, respectively. $HM_{tot,M}$ represented the total amount of the adsorbed heavy metal.

3.5. Distribution proportion of mechanisms contributions

The demineralized CMHCC was prepared by washing with 1 mol HCl solution, whose oxygenated functional groups were still preserved (Wang et al., 2022). Using the same conditions described, 20 mg demineralized CMHCC were added into three kinds of 20 mL $100\ \text{mg}\cdot\text{L}^{-1}$ heavy metal solutions individually. The adsorption capacity of precipitation with minerals (Q_{pre}), exchange with cation (Q_{exc}), complexation with acid functional groups (carboxyl and hydroxyl) (Q_{com}), and other potential mechanisms (Q_{oth}) were calculated (Wang et al., 2022). The contributions of different mechanisms were defined by following the ratios: Q_{pre}/Q_{tot} , Q_{exc}/Q_{tot} , Q_{com}/Q_{tot} , and Q_{oth}/Q_{tot} .

3.5.1. Contribution of the interaction with minerals

Contribution of the interaction with minerals (Q_{min} , $\text{mg}\cdot\text{g}^{-1}$) was calculated as Eq. (12).

$$Q_{min} = Q_{tot} - Q_{dem} \times Y \quad (12)$$

where, Q_{tot} ($\text{mg}\cdot\text{g}^{-1}$) was the total amount of three kinds of heavy metal adsorbed on the CMHCC, and Q_{dem} ($\text{mg}\cdot\text{g}^{-1}$) was the adsorbed amount of three kinds of heavy metal on the demineralized CMHCC, Y was the yield of demineralized CMHCC.

3.5.2. Contribution of the ion – exchange

The adsorption capacity attributed to ion – exchange (Q_{exc} , $\text{mg}\cdot\text{g}^{-1}$) was calculated from the net release of these cations. Specifically, the net amounts of cations released were calculated by subtracting the specific cation in the control group (CMHCC in deionized water) from the corresponding experimental group (CMHCC in heavy metal solutions). Since the substances containing K^+ and Na^+ often existed in the form of soluble compounds, while Ca^{2+} and Mg^{2+} were generally composed of

insoluble precipitates, this work optimized the previous research via measuring the contents of Ca^{2+} and Mg^{2+} to calculate (Eq. (13)).

$$Q_{exc} = Q_{Mg} + Q_{Ca} + Q_{Na} + Q_K \approx Q_{Mg} + Q_{Ca} \quad (13)$$

Here, Q_{Mg} and Q_{Ca} were the net release amount of Ca^{2+} and Mg^{2+} , respectively.

3.5.3. Contribution of the mineral precipitation

The contribution of mineral precipitation (Q_{pre} , $\text{mg}\cdot\text{g}^{-1}$) can be calculated as Eq. (14).

$$Q_{pre} = Q_{min} - Q_{exc} \quad (14)$$

3.5.4. Contribution of the complexation

The adsorption capacity resulting from complexation with the oxygenated functional groups (Q_{com} , $\text{mg}\cdot\text{g}^{-1}$) was estimated from the difference in pH before and after adsorption (Eq. (15)).

$$Q_{com} = Q_{pH} \times Y \quad (15)$$

where, Q_{pH} was the adsorbed heavy metal by complexation with oxygenated functional groups on demineralized CMHCC.

3.5.5. Contribution of other mechanisms

The amount of adsorption from other mechanisms (Q_{oth} , $\text{mg}\cdot\text{g}^{-1}$) was calculated as Eq. (16).

$$Q_{oth} = Q_{tot} - Q_{mi} - Q_{com} \quad (16)$$

4. Results and discussion

4.1. Characteristics of CMHCC

The basic elements of CMHCC were shown in Table S1. For CMHCC, the O/C ratio of CMHCC was 1.48, and the H/C ratio was 0.18, indicating the CMHCC exhibited good agronomic characteristics and fulfilled key quality criteria of $\text{H}/\text{C} < 0.70$ for soil carbon sequestration, as described by the European Biochar Certificate and the International Biochar Initiative (Yan et al., 2022). Noteworthy, the contents of phosphorus (P%) and sulfur element (S%) were 0.61 % and 1.69 %, respectively, which proved the existence of endogenous phosphorus and sulfur – containing functional groups in CMHCC. For CMHCC, the SSA was $11.78\ \text{m}^2\cdot\text{g}^{-1}$, and the average pore size was $837.94\ \text{\AA}$ (Table S1). The SSA is associated with physical properties and significantly affects the physical adsorption capacity (Shakya et al., 2022).

The SEM and SEM – EDS images were shown in Fig. 1. The layered porous structure riddled with micropores was presented on CMHCC, as biomass material contained cellulose (Anacleto et al., 2022). The ledge structure was related to pyrolysis temperature change (Adhikari et al., 2022), and CMHCC retained a part of the stereoscopic carbonaceous skeleton structure and bulk accumulation. Thus, the CMHCC may had good physical adsorption capacity. The CMHCC contained Ca, Mg, Si, and P (Fig. 1c–f). Moreover, Ca and P were distributed evenly on the surface of CMHCC, and Si and Mg were mainly distributed on the carbon skeleton.

The XRD spectra of CMHCC was depicted in Fig. 6a. CMHCC contained SiO_2 (26.6°) (PDF#70–2517). The substances included a combination of embedded metal cations (Ca^{2+} and Mg^{2+}) and anions (PO_4^{3-} and CO_3^{2-}), such as $\text{Ca}_3(\text{PO}_4)_2$ (PDF#09–0169), $\text{Mg}_3(\text{PO}_4)_2$ (PDF#48–1167), and CaCO_3 (PDF#70–0095) (Wu et al., 2020), which was consistent with SEM – EDS image (Fig. 1e). This indicated that CMHCC had the potential to adsorb heavy metal via ion – exchange and precipitation.

The FTIR spectra of CMHCC was depicted in Fig. 6b. The peak of $-\text{OH}$ ($3458\ \text{cm}^{-1}$), C–O stretching vibration peak ($1384\ \text{cm}^{-1}$), and the C–O–C peak ($876\ \text{cm}^{-1}$) were observed (Wang et al., 2019). Furthermore, the peak of CO_3^{2-} and PO_4^{3-} ($1415\ \text{cm}^{-1}$ and $1096\ \text{cm}^{-1}$) (Sun

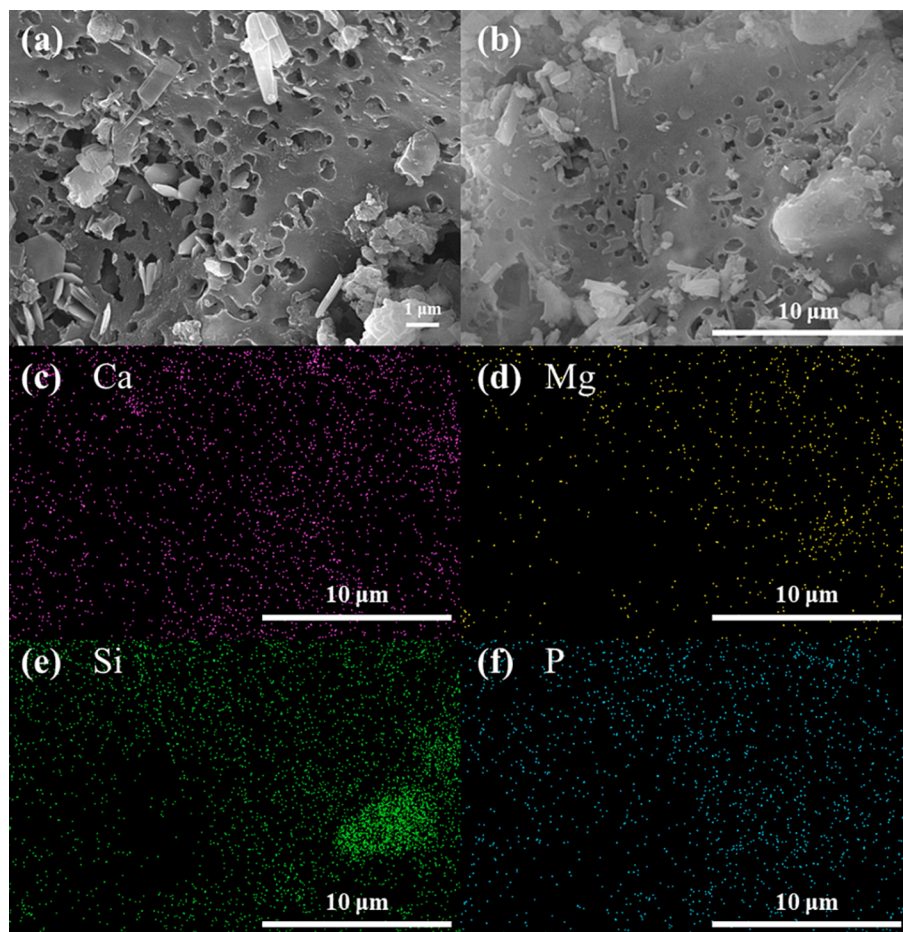


Fig. 1. SEM (a and b) and EDS (c–f) images of CMHCC.

et al., 2022), as well as the peak of Si–O–Si (1030 and 780 cm^{-1}) were observed (Kumaraswamy et al., 2021). These results indicated that CO_3^{2-} , PO_4^{3-} , and SiO_2 were retained in CMHCC, which was mutually verified with the above conclusion (Fig. 1 and Fig. 6a). Besides, the functional groups in CMHCC were so rich that they can be coordinated with heavy metal, indicating that CMHCC may adsorb heavy metal via formation of complexations (Du et al., 2022, Luo et al., 2022).

4.2. Adsorption performance

4.2.1. Kinetics model

The fitting results of kinetic model of CMHCC were shown in Table 1 and Fig. 2. In the adsorption processes of Pb(II) via CMHCC ($\text{pH} = 6$), the R^2 values of pseudo – first – order kinetic model and pseudo – second

Table 1
Table of fitting parameters of kinetic model and isotherm model of absorption.

Models	Parameters	Pb(II)	Cd(II)	Hg(II)
Pseudo – first – order kinetic model	Q_e ($\text{mg}\cdot\text{g}^{-1}$)	99.84	59.14	61.75
	k_1	0.43	2.22	1.91
	R^2	0.98	0.99	0.98
Pseudo – second – order kinetic model	Q_e ($\text{mg}\cdot\text{g}^{-1}$)	99.24	59.85	56.42
	K_2	6.27	0.03	0.85
	R^2	0.99	0.91	0.98
Langmuir model	Q_e ($\text{mg}\cdot\text{g}^{-1}$)	466.45	339.48	264.19
	K_L	2.95	6.18	4.19
	R^2	0.97	0.97	0.96
Freundlich model	n	1.34	1.98	2.30
	K_F	4.20	2.21	2.37
	R^2	0.96	0.94	0.98

– order kinetic model were 0.98 and 0.99, respectively, while those of adsorption processes of Hg(II) via CMHCC were 0.97 and 0.98, respectively. Thus, the adsorption processes of Pb(II) and Hg(II) were better fitted by pseudo – second – order kinetic model. This phenomenon may indicated that physisorption and chemisorption likely coexisted during adsorption of Pb(II) and Hg(II). On the contrary, the R^2 values of pseudo – first – order kinetic model and pseudo – second – order kinetic model in the adsorption of Cd(II) via CMHCC were 0.99 and 0.91, respectively, which indicated that physisorption dominated Cd(II) adsorption by CMHCC (Chowdhury et al., 2022).

The equilibrium time of absorption of three kinds of heavy metal by CMHCC was distinct. When $\text{pH} = 6$, the equilibrium time of Pb(II) adsorption was about 3 h, and that of Hg(II) adsorption was approximately 2 h, while that of Cd(II) adsorption was about 6 h. The different adsorption equilibrium time may be due to the dominated adsorption, the physisorption was reversible and slow (Zhang et al., 2022a), which corresponded to the kinetic model fitting results mentioned above (Fig. 2). Furthermore, the equilibrium time of absorption was attributed to the same valency metal ions having different electronegativities and atomic radii. The smaller the hydrated radius and higher electronegativity is, the greater the affinity in the sorption process (Xiao et al., 2020). Pb(II) might have preferential sorption compared with Cd(II), for the electronegativity values and hydrated radius of Cd(II) are 0.69 and 4.26 \AA , respectively, while those of Pb(II) are 2.33 and 4.01 \AA , respectively.

4.2.2. Isothermal model

The fitting results of isothermal adsorption model were presented in Fig. 2. The R^2 values of the Langmuir model and Freundlich model for Pb

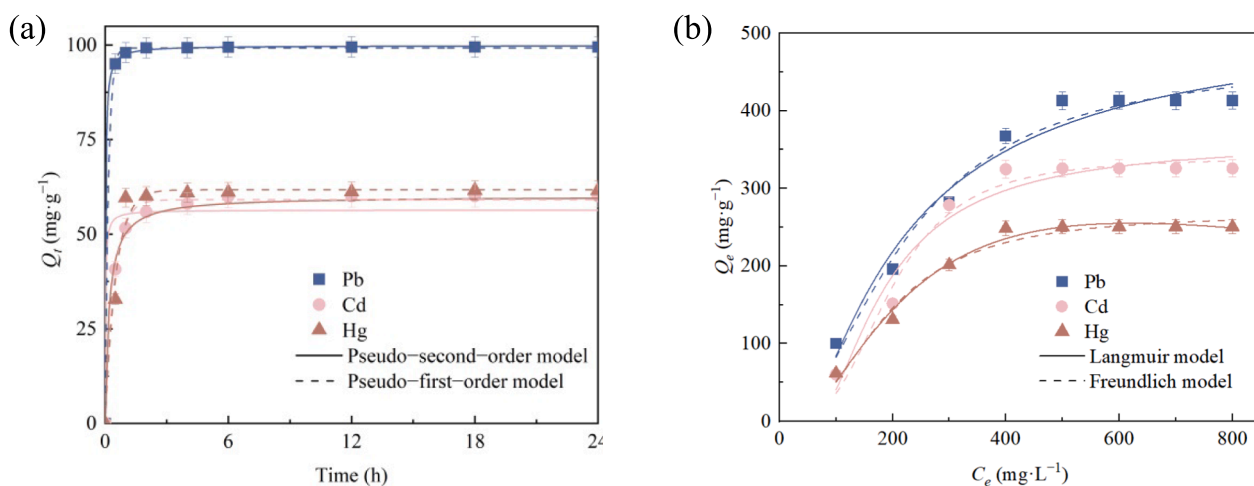


Fig. 2. Fitting parameters of kinetic model (a) and isotherm model (b) of absorption. Experiment condition: [dosage] = 1 g·L⁻¹, [temperature] = 25 °C, [pH] = 6.0.

(II) adsorption by CMHCC were 0.97 and 0.96, respectively, and those for Cd(II) adsorption were 0.97 and 0.94, respectively. Clearly, the Langmuir model fit the adsorption of Pb(II) and Cd(II) better. Moreover, for Hg(II) adsorption, the R^2 values of the Langmuir model and Freundlich model were both 0.98, thus, the Langmuir model fit the adsorption of Hg(II) better. Therefore, the adsorption of Pb(II), Cd(II), and Hg(II) by CMHCC were monolayer adsorption, indicating that single – layer surface adsorption might be the dominant process governing the sorption process (Xu et al., 2022). The corresponding Q_e of Pb(II), Cd(II), and Hg(II) on CMHCC were 466.45, 339.48, and 264.19 mg·g⁻¹, respectively. CMHCC exhibited excellent sorption properties than many reported sorbents including hydrochars and some carbon – based materials (Table S3).

4.2.3. Effect of pH

The adsorptions of CMHCC on three kinds of heavy metal were affected by the pH (Fig. 3a). In general, under acidic conditions (pH from 2 to 6), the adsorption effect of CMHCC on three kinds of heavy metal enhanced with the increasing of solution pH. As shown in Figure S1, the surface of CMHCC was positively charged when pH = 2, while that was relatively negative charged at pH = 4. The more acidic the solution, the more positive charge on the surface of adsorbent, so that the adsorbent was easier to be protonated, which weakened the adsorption effect. As the pH continued to increase to 6, the adsorption sites became less positively charged, and more sorption sites could be deprotonated, enabling complexation with more Pb(II), Cd(II), and Hg(II).

When the pH increased from 2 to 6, the Q_e enhanced 31 times (3.20 vs. 99.49 mg·L⁻¹), thus, the adsorption of Pb(II) by CMHCC was

significantly affected by pH. From this we can infer that electrostatic attraction made a great contribution to adsorption on Pb(II).

4.3. Phosphorus leaching performance

Since the material of CMHCC was cow manure, CMHCC contained endogenous phosphorus. While the endogenous phosphorus releases by CMHCC were different between the deionized water and heavy metal solutions (Fig. 3b). After CMHCC was placed in deionized water for 24 h, the phosphorus contents were 4.81, 4.14, and 4.01 mg·g⁻¹ at pH = 2, 4 and 6, respectively. The acid solution promoted the release, which may be due to carbon skeletons were more dissolved, increasing the contact area to release (Lonappan et al., 2020).

In the process of adsorption of Pb(II) via CMHCC, the residual phosphorus content decreased with the increase of pH, and it was noteworthy that the sharp trend of residual phosphorus content was the same as that of Q_e . It can be inferred that the endogenous phosphorus released acted on the removal of Pb(II) (Wang et al., 2023b). As shown in Table S2, the ratio (Q_e : Content of phosphorus consumed) was about 3 (3.13 and 3.51 for pH = 4 and pH = 6). Phosphoric acid, hydrogen phosphate and other anions formed when the endogenous phosphorus was released, and they can combine with Pb(II), resulting in the reduction of phosphorus content.

In the process of adsorption of Cd(II) via CMHCC, the residual phosphorus content decreased slightly with the increase of pH. It can be inferred that the endogenous phosphorus had the effect on adsorption of Cd(II), but co-precipitation were not the main mechanism of Cd(II) removal.

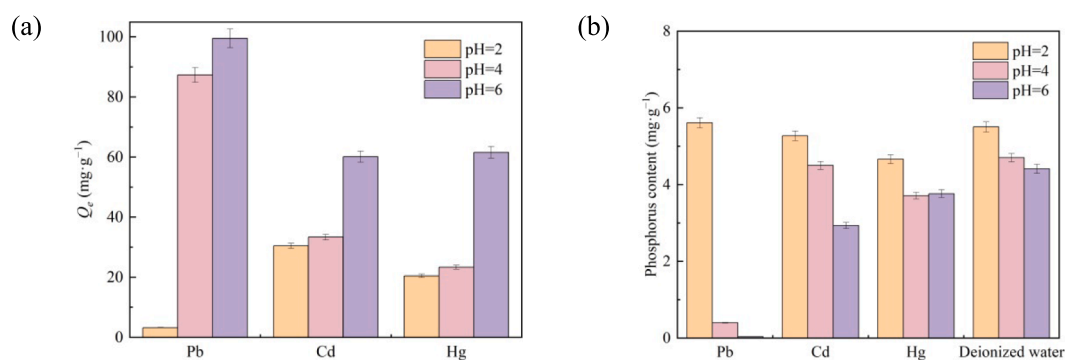


Fig. 3. Effect of pH on adsorption (a) and endogenous phosphorus leaching performance (b). Experiment condition: [dosage] = 1 g·L⁻¹, [temperature] = 25 °C, [time] = 24 h.

In the process of adsorption of Hg(II) via CMHCC, When pH increased from 4 to 6, and the Q_e increased from 20.44 to 61.57 $\text{mg}\cdot\text{g}^{-1}$, an increase of 264 %. But, the residual phosphorus content in solution was almost unchanged. It can be inferred that endogenous phosphorus hardly contributed to the removal, while OH^- may play a major role (Song et al., 2023).

4.4. Characterization of CMHCC@HM

4.4.1. Analysis of phosphorus morphology

The phosphorus in solution was denoted as R_p , and the phosphorus on CMHCC@HM was denoted as BC_p , which included the endogenous phosphorus undissolved and the phosphorus that binded with heavy metal and then attached to the surface of hydrochar. The morphology of BC_p was analyzed (Fig. 4a), which including L - P, RSP, Fe/Al - P, and Ca - P according to four - step continuous extraction method mentioned above.

Phosphorus in the form of L - P was exchangeable, and L - P was easily diffused into solution and used by organisms. Phosphorus in the form of RSP was considered as occluded phosphate. RSP generally coated by Fe_2O_3 , and was biologically unavailable (Tang et al., 2018). Phosphorus in the form of Fe/Al - P can be bioavailable under certain conditions, so Fe/Al - P was potential activated. Phosphorus in the form of Ca - P was an insoluble substance and difficult to be used by organisms, and Ca - P was mostly phosphate of calcium such as apatite phosphorus (Zhang et al., 2020b).

The phosphorus on CMHCC mainly existed in the form of L - P, and the rest almost can be classified into two categories: RSP and Ca - P. This indicated that phosphorus on CMHCC existed in an unstable state and easily entered the water or be used. For CMHCC@Pb, the phosphorus mostly existed in the form of Ca - P. Phosphorus of CMHCC was converted from L - P to Ca - P during the Pb(II) adsorption. Phosphate combined with Pb^{2+} to form insoluble precipitates, such as $\text{Pb}_5(\text{PO}_4)\text{Cl}$ and $\text{Pb}_3(\text{PO}_4)_2$. The significant transformation of phosphorus morphology during the adsorptions of Cd(II) and Hg(II) was the increase of Fe/Al - P, for Fe/Al - P contents of CMHCC@Cd and CMHCC@Hg were 175 and 174 times higher than that of CMHCC, respectively. This indicated that REDOX reaction was involved in the removal of heavy metal. Besides, Ca - P content of CMHCC@Cd was increased by 224 %, indicating that co-precipitation was involved in removal of Cd(II), but the proportion was not as large as that in Pb(II) removal. The removal of three heavy metal by CMHCC had a commonality, that is, the proportion of bioavailable phosphorus decreased. This may indicate that using CMHCC to remove heavy metal not only had great adsorption effect, but also little harm of eutrophication caused by endogenous phosphorus release.

4.4.2. Analysis of heavy metal' morphology

The environmental behavior and ecological effect were not evaluated by total contents of heavy metal in hydrochar, but heavy metal' morphology were the key factors to determine the impact on the environmental ecosystems. As shown in Fig. 4b, heavy metal' morphologies of CMHCC@HM were extracted, and the HM_{ex} , HM_{ac} , and HM_{ge} represented the exchangeable, acid soluble, and generally stable heavy metal, respectively. The HM_{ex} was sensitive to environment, easy to migrate and transform, and can be absorbed by plants. The HM_{ac} was harmful to the environment, and its release activity was enhanced when the environmental conditions become acidic. The HM_{ge} was insoluble and had an impact on organisms only through chemical reactions into soluble substances.

After adsorption of heavy metal on CMHCC, three kinds of heavy metal mainly existed in the form of HM_{ge} . For CMHCC@Pb, although HM_{ge} had the largest proportion, accounting for 74.83 %, HM_{ex} also accounted for 24.08 %. This indicated that the heavy metal biological risk of CMHCC@Pb was high. For CMHCC@Cd, HM_{ge} had the largest proportion accounted for 93.25 %, indicating that the heavy metal biological risk of CMHCC@Cd was low. Though HM_{ge} of CMHCC@Cd had the largest proportion, Ca - P did not, which was speculated that the insoluble and stable precipitation formed may was mainly carbonate rather than phosphate.

4.4.3. Characterization

To clarify the interaction mechanisms between CMHCC and three kinds of heavy metal, a series of characterizations were performed and the results were discussed in detail. The SEM and SEM - EDS images of CMHCC@HM were shown in Fig. 5. The SEM analysis clearly showed that the difference in physical microstructure of the CMHCC and CMHCC@HM (Subhashish et al., 2022). Compared with CMHCC, the pore structures of CMHCC@HM were less. The surface plane of CMHCC exhibited heterogeneous textural properties, with a strong porous structure. And the presence of these cavities gave the CMHCC capacity for biosorptions of heavy metal (Subhashish et al., 2023). In fact, these heavy metal salts filled the holes. The surface of CMHCC@Pb was rough and had many small crystalline materials attached to it (Fig. 5a). On the contrary, the surface of CMHCC@Hg had obvious massive crystalline material. The EDS images showed that the Pb and P were evenly distributed on the surface of on CMHCC@Pb (Fig. 5b - c), and the distribution of Pb was similar to that of P. This phenomenon was similar to that of CMHCC@Cd (Fig. 5e - f). However, on the surface of CMHCC@Hg, the P still distributed dispersedly, the Hg concentrated on crystal particles, which was not similar to that of P (Fig. 5h - i). According to this phenomenon, we speculated that in adsorption of Hg(II) by CMHCC, endogenous phosphorus was scarcely any involved, and the crystal particles formed after adsorption were not phosphate substances.

The XRD spectra of CMHCC@HM was shown in Fig. 6. For

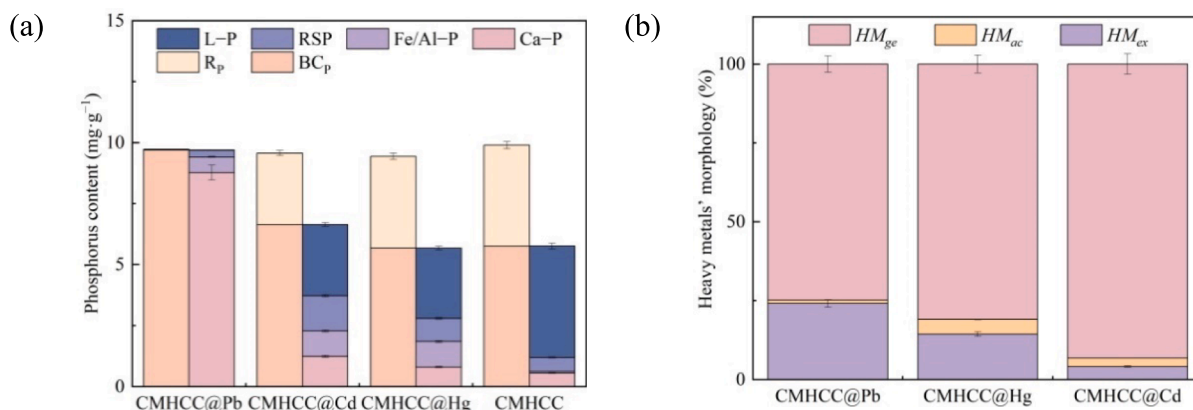


Fig. 4. Analysis of different forms of phosphorus and heavy metal in CMHCC@HM. a: analysis of phosphorus morphology; b: analysis of heavy metal' morphology.

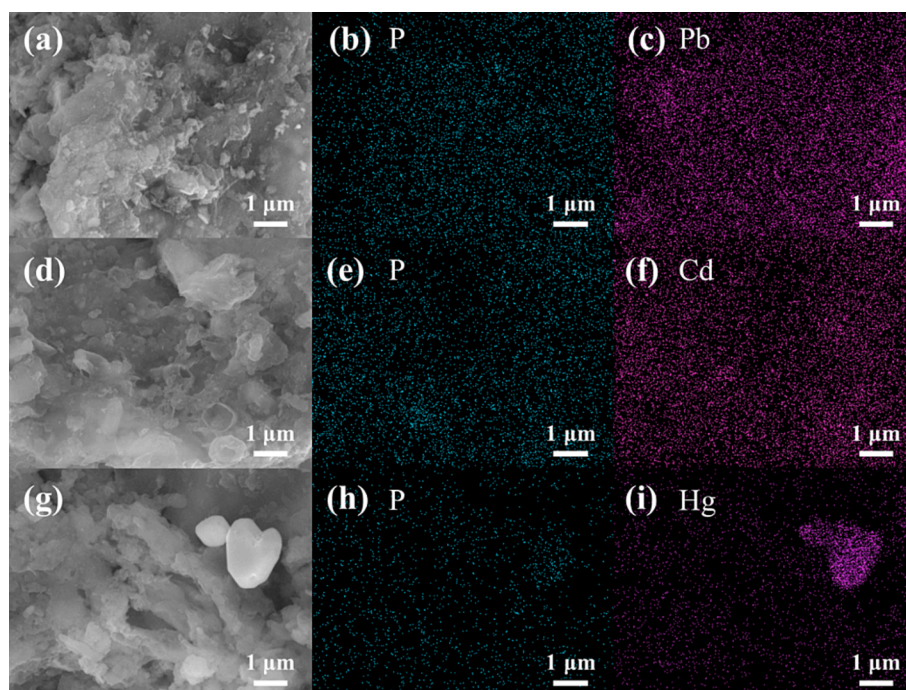


Fig. 5. SEM and EDS images of CMHCC@HM. a: SEM images of CMHCC@Pb; b–c: EDS images for Pb and P of CMHCC@Pb; d: SEM images of CMHCC@Cd; e–f: EDS images for Cd and P of CMHCC@Cd; g: SEM images of CMHCC@Hg; h–i: EDS images for Hg and P of CMHCC@Hg.

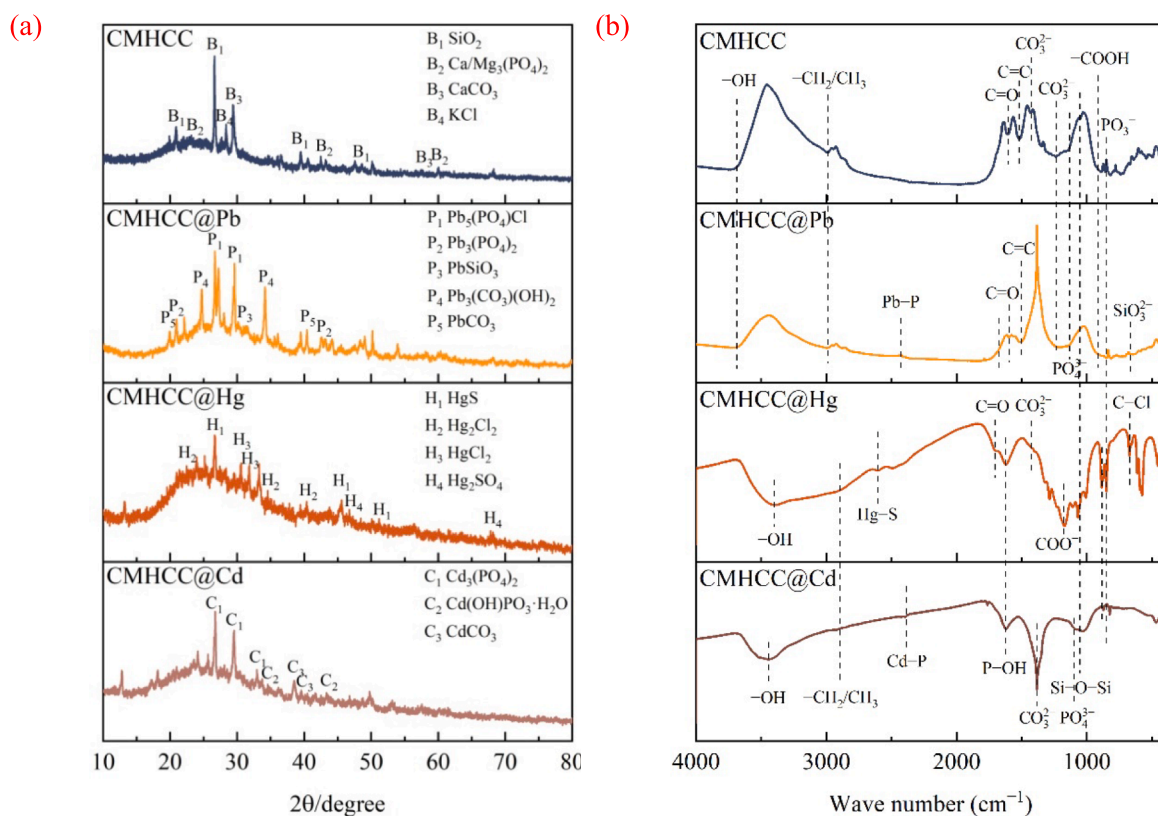


Fig. 6. Characterization of CMHCC@HM and CMHCC. a: XRD spectra, b: FTIR spectra.

CMHCC@Pb, the characteristic peaks at 20.8°, 27.28°, and 42° represented Pb₃(PO₄)₂ (PDF#73–0834), which confirm that endogenous phosphorus was involved in the removal of Pb(II) (Li et al., 2022). The

characteristic peak at 26.6° and 40° represented PbSiO₃ (PDF#74–1101) and PbCO₃ (PDF#85–1088), respectively, confirming the role of precipitation. Besides, PbCO₃ ($K_{sp} = 3.3 \times 10^{-14}$) was less

soluble than CaCO_3 ($K_{sp} = 2.8 \times 10^{-9}$) and MgCO_3 ($K_{sp} = 2.6 \times 10^{-5}$) (Liu et al., 2022), hence, the removal mechanism of Pb(II) may involve ion – exchange. Moreover, $\text{Pb}_3(\text{CO}_3)_2(\text{OH})_2$ (PDF#72–1144) verified hydroxyl group participated in adsorption (Qu et al., 2022), which suggested that the functional groups on CMHCC may be complexed with Pb(II) for adsorption. The $\text{Pb}_5(\text{PO}_4)_3\text{Cl}$ verified precipitation participated in adsorption (Ge et al., 2022). For CMHCC@Hg, the ion – exchange and physicochemical for the formation of Hg_2Cl_2 (Kong et al., 2011). For CMHCC@Cd, co-precipitation and complexation involved in the adsorption for the formation of $\text{Cd}(\text{OH})\text{PO}_3 \cdot \text{H}_2\text{O}$ and $\text{Cd}_3(\text{PO}_4)_2$ (Zhang et al., 2020a), and ion – exchange also involved in the adsorption possibly for $\text{Cd}_3(\text{PO}_4)_2$ existed (Wang et al., 2022).

The FTIR spectra of CMHCC@HM was shown in Fig. 6b. For CMHCC@Pb, the peak value of Si–O–Si disappeared, possibly due to the cation– π bond interaction existed (Feng et al., 2023). The peaks of CO_3^{2-} and PO_4^{3-} existed, possibly due to precipitation $\text{Pb}_3(\text{CO}_3)_2(\text{OH})_2$ and $\text{Pb}_3(\text{PO}_4)_2$ (Pei et al., 2021), which confirming the previous speculation (Fig. 6a). The Pb–P peak at 2300 – 2450 cm^{-1} appeared, indicating the presence of phosphates of heavy metal (Xia et al., 2020). The band at 665 cm^{-1} was indicative of SiO_3^{2-} (Tang et al., 2015).

For CMHCC@Hg, the –OH group peak shifted, presumably the hydroxyl group complexed with Hg(II), and the peak of –COOH disappeared, which possibly due to the complexation of Hg(II) with phenolic hydroxyl (CO^-) and carboxylic (COO^-) group (Xu et al., 2016). The COO^- peak at 1159 cm^{-1} appeared, proving the formation of complexations. The C = C and C = O peaks shifted, which possibly due to the cation – π interaction (Liu et al., 2018). The Hg–S peak at 2550 – 2650 cm^{-1} appeared, indicating the presence of heavy metal sulfides, such as HgS (Xia et al., 2020). The C–S bond formed on surface hydrochar led to formation of HgS by formation of complexations based on Hard – Soft and Acid Base (HSAB) theory. Without the addition of sulfur, Hg adsorption normally occurred at carboxyl and carbonyl groups, forming HgO and HgCl_2 (Fig. 6a) (Jeon et al., 2020).

For CMHCC@Cd, the –OH group peak shifted, which presumably due to the hydroxyl group complexed with Cd(II). The peaks of PO_3^- , PO_4^{3-} and CO_3^{2-} shifted, which possibly due to the precipitation and formation of complexations for the formation of $\text{Cd}(\text{OH})\text{PO}_3 \cdot \text{H}_2\text{O}$, $\text{Cd}_3(\text{PO}_4)_2$, and Cd_3CO_3 (Zhang et al., 2020a). The peak of Cd–P peak at 2300 – 2450 cm^{-1} appeared, indicating the presence of phosphates of heavy metal. The shift of $-\text{CH}_2/\text{CH}_3$ group may due to the H^+ provided from $-\text{CH}_2/\text{CH}_3$ had an ion – exchange reaction with Cd(II) (Ge et al., 2022). And the CMHCC adsorb Cd (II) via the role of O-containing groups, mainly by reactions of organic complexation (Zhang et al., 2022b).

4.5. Mechanisms for contributions

The mechanisms of adsorptions on three kinds of heavy metal were

quantitatively analyzed and the results were shown in Fig. 7. The main adsorption mechanism was various when CMHCC was used to adsorb Pb (II), Cd(II), and Hg(II). Ion – exchange was considered as the dominant mechanism for Pb(II) and Cd(II) adsorptions on CMHCC, the contribution rates of ion – exchange being equivalent to 55.89 and 41.59 $\text{mg} \cdot \text{g}^{-1}$, which accounted for 56.17 % and 69.18 % of the total adsorption capacity, respectively (Fig. 7). The contribution rates of co-precipitation accounted for 16.65 % and 18.70 % of the total adsorption capacity of Pb(II) and Cd(II) adsorptions on CMHCC, respectively, while contribution rates of formation of complexations accounted for 24.97 % and 5.98 %, respectively (Fig. 7b). For CMHCC@Cd, HM_{ge} had the largest proportion but Ca – P did not, thus, it was speculated that insoluble and stable precipitations were mainly carbonate rather than phosphate. For CMHCC@Pb, HM_{ge} and Ca – P both had the largest proportion, thus, it was speculated that precipitations were mainly phosphate.

The precipitation reaction was dominated for Pb(II) and Cd(II) (Su et al., 2022). On the contrary, formation of complexations with the oxygenated functional groups was considered as the dominant mechanism for Hg(II) adsorption on CMHCC, and the contribution rate of complexation accounted for 65.17 % of the total adsorption capacity, but the contribution rate of precipitation only accounted for 7.04 %. Therefore, phosphate contributed little to the removal of Hg(II).

5. Conclusion

In this work, the biochar synthesized from cow manure was proved to have adsorption effects for Pb(II), Cd(II), and Hg(II) in solutions, while the adsorption mechanisms were investigated qualitatively and quantitatively. The results indicated that the potential CMHCC application for removal of Pb(II), Cd(II), and Hg(II) in solutions. However, when CMHCC adsorbed heavy metal, the adsorption mode was different.

The physisorption and chemisorption likely coexisted during adsorption of Pb(II) and Hg(II), while physisorption dominated Cd(II) adsorption by CMHCC. The adsorption data of Pb(II), Cd(II), and Hg(II) can be described by the Langmuir isothermal model with the capacity as 466.45, 339.48, and 264.19 $\text{mg} \cdot \text{g}^{-1}$, respectively, demonstrating that the adsorption of Pb(II), Cd(II), and Hg(II) by CMHCC were likely monolayer adsorption.

Ion – exchange was considered as the dominant mechanism for Pb (II) and Cd(II) adsorptions on CMHCC, the contribution rates of ion – exchange was accounted for 55.89 and 41.59 $\text{mg} \cdot \text{g}^{-1}$, which accounted for 56.17 % and 69.18 % of the total adsorption capacity, respectively. In the case of CMHCC@Cd, the insoluble and stable precipitations formed after adsorption were mainly carbonate. However, phosphate precipitation was the main product for CMHCC@Pb. The endogenous phosphorus of CMHCC played crucial roles in the adsorption of Pb(II)

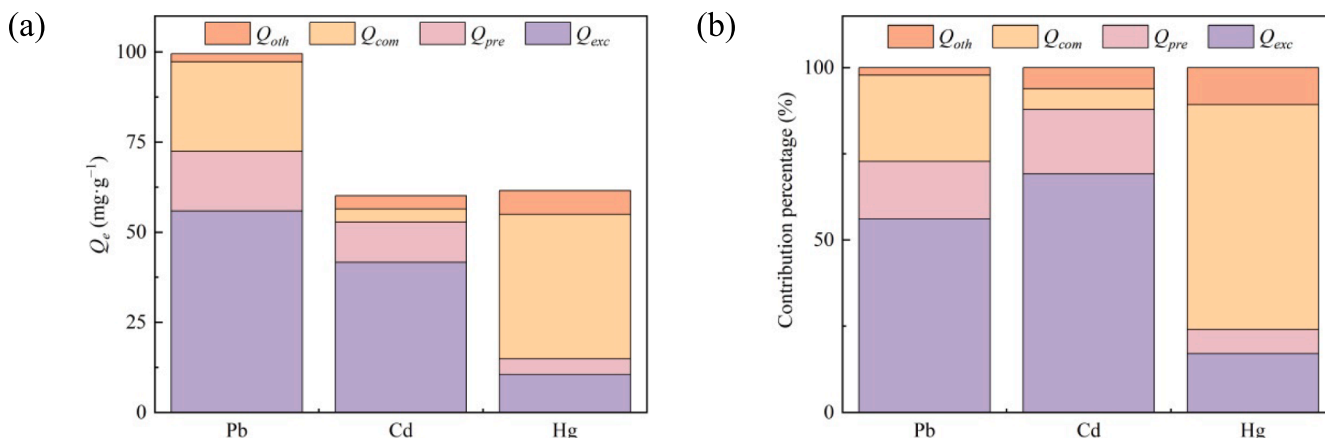


Fig. 7. Analysis of mechanisms contributions.

than that of Cd(II). On the contrary, formation of complexations with the oxygenated functional groups was considered as the dominant mechanism for Hg(II) adsorption on CMHCC (65.17 %), but the contribution rate of co-precipitation only accounted for 7.04 %. To sum up, the endogenous phosphorus of CMHCC contributed greatly to the adsorption of Pb(II), but had little effect on the removal of Hg(II).

Furthermore, the biological risks of CMHCC adsorbing three kinds of heavy metal were different. Using CMHCC to remove three kinds of heavy metal not only had great adsorption effect, but also little harm of eutrophication caused by endogenous phosphorus release for the proportion of bioavailable phosphorus decreased. After adsorption of heavy metal on CMHCC, three kinds of heavy metal mainly existed in the form of HM_{ge} . The HM_{ex} of CMHCC@Pb accounted for 24.08 %, indicating that CMHCC@Pb had the highest heavy metal biological risk, followed by CMHCC@Cd and CMHCC@Hg. These results are helpful in providing solutions for ecological treatment of cow manure and optimizing the selection of adsorption objects of phosphorus containing biomass. The biotoxicity analysis of CMHCC@HM was beneficial to evaluate the application feasibility.

Funding: This work was supported by the National Natural Science Foundation of China [22264025], the Natural Science Foundation of China [52100147], the Yunnan Plateau Characteristics of Bio-fertilizer [202202AE090025], Applied Basic Research Foundation of Yunnan Province [202201AS070020, 202201AU070061], and the Science and Technology Research Project of Education Department of Jiangxi Province [DA202102159].

Institutional Review Board Statement: "Not applicable" for studies not involving humans or animals.

CRedit authorship contribution statement

Yi Wen: Formal analysis. **Dingxiang Chen:** Data curation, Software, Methodology. **Yong Zhang:** Data curation, Investigation, Methodology. **Huabin Wang:** Supervision, Writing – review & editing. **Rui Xu:** Funding acquisition, Resources, Supervision.

Declaration of competing interest

The authors declare that they have no known competing financial interests or personal relationships that could have appeared to influence the work reported in this paper.

Appendix A. Supplementary data

Supplementary data to this article can be found online at <https://doi.org/10.1016/j.arabjc.2023.105530>.

References

- Adhikari, S., Timms, W., Mahmud, M.A.P., 2022. Optimising water holding capacity and hydrophobicity of biochar for soil amendment—A review. *Science of the Total Environment*. 851, 158043 <https://doi.org/10.1016/j.scitotenv.2022.158043>.
- Anacleto, T.M., Oliveira, H.R., Diniz, V.L., et al., 2022. Boosting manure biogas production with the application of pretreatments: A meta-analysis. *Journal of Cleaner Production*. 362, 132292 <https://doi.org/10.1016/j.jclepro.2022.132292>.
- Bao, Z., Shi, C., Tu, W., et al., 2022. Recent developments in modification of biochar and its application in soil pollution control and ecoregulation. *Environmental Pollution*. 313, 120184 <https://doi.org/10.1016/j.envpol.2022.120184>.
- Chen, G., Wang, J., Yu, F., et al., 2022. A review on the production of P-enriched hydro/bio-char from solid waste: Transformation of P and applications of hydro/bio-char. *Chemosphere*. 301, 134646 <https://doi.org/10.1016/j.chemosphere.2022.134646>.
- Chowdhury, I.R., Chowdhury, S., Mazumder, M.A.J., et al., 2022. Removal of lead ions (Pb²⁺) from water and wastewater: a review on the low-cost adsorbents. *Applied Water Science*. 12, 185. <https://doi.org/10.1007/s13201-022-01703-6>.
- Du, H., Xi, C., Tang, B., et al., 2022. Performance and mechanisms of NaOH and ball-milling co-modified biochar for enhanced the removal of Cd²⁺ in synthetic water: A combined experimental and DFT study. *Arabian Journal of Chemistry*. 14 (5), 1030119. <https://doi.org/10.1016/j.arabjc.2021.103119>.
- Feng, C., Huang, M., Huang, C.P., 2023. Specific chemical adsorption of selected divalent heavy metal ions onto hydrous γ -Fe₂O₃-biochar from dilute aqueous solutions with

- pH as a master variable. *Chemical Engineering Journal*. 451, 138921 <https://doi.org/10.1016/j.cej.2022.138921>.
- Ge, Q., Tian, Q., Hou, R., et al., 2022. Combing phosphorus-modified hydrochar and zeolite prepared from coal gangue for highly effective immobilization of heavy metal in coal-mining contaminated soil. *Chemosphere*. 291, 132835 <https://doi.org/10.1016/j.chemosphere.2021.132835>.
- Hieltsjes, A.H.M., Lijklema, L., 1980. Fractionation of Inorganic Phosphates in Calcareous Sediments. *Soil Science Society of America Journal*. 9, 405–407. <https://doi.org/10.2136/sssaj1971.03615995003500020023x>.
- Jeon, C., Solis, K.L., An, H.R., et al., 2020. Sustainable removal of Hg(II) by sulfur-modified pine-needle biochar. *Journal of Hazardous Materials*. 388, 122048 <https://doi.org/10.1016/j.jhazmat.2020.122048>.
- Jun, H., Liu, J., Liu, Y., 2005. Study on the difference of phosphorus fractionations between the sediment and the suspended matter. *Acta Scientiae Circumstantiae*. 25, 1517–1522.
- Kong, H., He, J., Gao, Y., et al., 2011. Cosorption of Phenanthrene and Mercury(II) from Aqueous Solution by Soybean Stalk-Based Biochar. *Journal of Agricultural and Food Chemistry*. 59, 12116–12123. <https://doi.org/10.1021/jf202924a>.
- Kumar, M., Nandi, M., Pakshirajan, K., 2021. Recent advances in heavy metal recovery from wastewater by biogenic sulfide precipitation. *Journal of Environmental Management*. 278, 111555 <https://doi.org/10.1016/j.jenvman.2020.111555>.
- Kumar, A., Singh, E., Mishra, R., et al., 2022. Biochar as environmental armour and its diverse role towards protecting soil, water and air. *Science of the Total Environment*. 806, 150444 <https://doi.org/10.1016/j.scitotenv.2021.150444>.
- Kumaraswamy, R.V., Saharan, V., Kumari, S., et al., 2021. Chitosan-silicon nanofertilizer to enhance plant growth and yield in maize (*Zea mays* L.). *Plant Physiology and Biochemistry*. 159, 53–66. <https://doi.org/10.1016/j.plaphy.2020.11.054>.
- Li, H., Jiang, Q., Zhang, J., et al., 2022. Synchronization adsorption of Pb(II) and Ce(III) by biochar supported phosphate-doped ferrihydrite in aqueous solution: Adsorption efficiency and mechanisms. *Colloids and Surfaces a: Physicochemical and Engineering Aspects*. 648, 129230 <https://doi.org/10.1016/j.colsurfa.2022.129230>.
- Li, J., Yu, S., Hong, B., et al., 2023. Spatial effects of urban green infrastructure on instream water quality assessed by chemical and sensory indicators. *Science of the Total Environment*. 858, 160088 <https://doi.org/10.1016/j.scitotenv.2022.160088>.
- Liu, M., Hu, B., Zhang, C., et al., 2022. Effect of sodium silicate on the flotation separation of chalcopyrite and galena using sodium sulfite and sulfonated lignin as depressant. *Minerals Engineering*. 182, 107563 <https://doi.org/10.1016/j.mineng.2022.107563>.
- Liu, P., Ptacek, C.J., Elena, K.M.A., et al., 2018. Evaluation of mercury stabilization mechanisms by sulfurized biochars determined using X-ray absorption spectroscopy. *Journal of Hazardous Materials*. 347, 114–122. <https://doi.org/10.1016/j.jhazmat.2017.12.051>.
- Liu, X., Yin, H., Liu, H., et al., 2023. Multicomponent adsorption of heavy metal onto biogenic hydroxyapatite: Surface functional groups and inorganic mineral facilitating stable adsorption of Pb(II). *Journal of Hazardous Materials*. 443, 130167 <https://doi.org/10.1016/j.jhazmat.2022.130167>.
- Lonappan, L., Liu, Y., Rouissi, T., et al., 2020. Development of biochar-based green functional materials using organic acids for environmental applications. *Journal of Cleaner Production*. 244, 118841 <https://doi.org/10.1016/j.jclepro.2019.118841>.
- Long, Z., Ji, Z., Pei, Y., 2023. Characteristics and distribution of phosphorus in surface sediments of a shallow lake. *Journal of Environmental Sciences*. 124, 50–60. <https://doi.org/10.1016/j.jes.2021.10.012>.
- Luo, Q., Chen, D., Cui, T., et al., 2022. Selenium elimination via zero-valent iron modified biochar synthesized from tobacco straw and copper slag: Mechanisms and agro-industrial practicality. *Frontiers in Bioengineering and Biotechnology*. 10, 1054801. <https://doi.org/10.3389/fbioe.2022.1054801>.
- Ning, K., Gong, K., Chen, H., et al., 2022. Lead stabilization in soil using P-modified biochars derived from kitchen waste. *Environmental Technology and Innovation*. 28, 102953 <https://doi.org/10.1016/j.eti.2022.102953>.
- Pei, L., Yang, F., Xu, X., et al., 2021. Further reuse of phosphorus-laden biochar for lead sorption from aqueous solution: Isotherm, kinetics, and mechanism. *Science of the Total Environment*. 792, 148550 <https://doi.org/10.1016/j.scitotenv.2021.148550>.
- Qiu, B., Tao, X., Wang, H., et al., 2021. Biochar as a low-cost adsorbent for aqueous heavy metal removal: A review. *Journal of Analytical and Applied Pyrolysis*. 155, 105081 <https://doi.org/10.1016/j.jaap.2021.105081>.
- Qu, J., Wei, S., Liu, Y., et al., 2022. Effective lead passivation in soil by bone char/CMC-stabilized FeS composite loading with phosphate-solubilizing bacteria. *Journal of Hazardous Materials*. 423, 127043 <https://doi.org/10.1016/j.jhazmat.2021.127043>.
- Shakya, A., Vithanage, M., Agarwal, T., 2022. Influence of pyrolysis temperature on biochar properties and Cr(VI) adsorption from water with groundnut shell biochars: Mechanistic approach. *Environmental Research*. 215, 114243 <https://doi.org/10.1016/j.envres.2022.114243>.
- Song, W., Zhang, X., Zhang, L., et al., 2023. Removal of various aqueous heavy metals by polyethylene glycol modified MgAl-LDH: Adsorption mechanisms and vital role of precipitation. *Journal of Molecular Liquids*. 375 (1), 121386 <https://doi.org/10.1016/j.molliq.2023.121386>.
- Su, X., Chen, Y., Li, Y., et al., 2022. Enhanced adsorption of aqueous Pb(II) and Cu(II) by biochar loaded with layered double hydroxide: Crucial role of mineral precipitation. *Journal of Molecular Liquids*. 357 (1), 119083 <https://doi.org/10.1016/j.molliq.2022.119083>.
- Subhashish D., Anduri S., G.T.N. V., et al. 2022. Synthesis and characterization of mango leaves biosorbents for removal of iron and phosphorus from contaminated water. *Applied Surface Science Advances*. 11, 100292. <https://doi.org/10.1016/j.apsadv.2022.100292>.

- Subhshish, D., G.T.N. V., A.V. P., et al. 2023. Performances of plant leaf biosorbents for biosorption of phosphorous from synthetic water. *Cleaner Materials*. 8, 100191. [10.1016/j.clema.2023.100191](https://doi.org/10.1016/j.clema.2023.100191).
- Sun, Z., Wang, X., Xia, S., et al., 2022. Treatment of Pb(II) pollution in livestock wastewater by MgFe₂O₄ modified manure-biochar derived from livestock itself: Special role of endogenous dissolved organic matter and P species. *Chemical Engineering Journal*. 446, 137068 <https://doi.org/10.1016/j.cej.2022.137068>.
- Szogi, A.A., Takata, V.H., Shumaker, P.D., 2020. Chemical Extraction of Phosphorus from Dairy Manure and Utilization of Recovered Manure Solids. *Agronomy*. 10, 1725. <https://doi.org/10.3390/agronomy10111725>.
- Tang, W., Huang, H., Gao, Y., et al., 2015. Preparation of a novel porous adsorption material from coal slag and its adsorption properties of phenol from aqueous solution. *Materials and Design*. 88, 1191–1200. <https://doi.org/10.1016/j.matdes.2015.09.079>.
- Tang, X., Wu, M., Li, R., 2018. Phosphorus distribution and bioavailability dynamics in the mainstream water and surface sediment of the Three Gorges Reservoir between 2003 and 2010. *Water Research*. 145, 321–331. <https://doi.org/10.1016/j.watres.2018.08.041>.
- Teribebe, T., Costa, M.E.G., Sales da Silva, C.D.S., et al., 2023. Hydrothermal carbonization of corn stover: Structural evolution of hydro-char and degradation kinetics. *Energies*. 16 (7), 3217. <https://doi.org/10.3390/en16073217>.
- Wang, Q., Duan, C., Xu, C., et al., 2022. Efficient removal of Cd(II) by phosphate-modified biochars derived from apple tree branches: Processes, mechanisms, and application. *Science of the Total Environment*. 819, 152876 <https://doi.org/10.1016/j.scitotenv.2021.152876>.
- Wang, H., Duan, R., Ding, L., et al., 2023a. Magnetic hydrochar derived from waste lignin for thallium removal from wastewater: Performance and mechanisms. *Bioresource Technology*. 374, 128736 <https://doi.org/10.1016/j.biortech.2023.128736>.
- Wang, F., Li, J., Su, Y., et al., 2019. Adsorption and recycling of Cd(II) from wastewater using straw cellulose hydrogel beads. *Journal of Industrial and Engineering Chemistry*. 80, 361–369. <https://doi.org/10.1016/j.jiec.2019.08.015>.
- Wang, H., Wen, Y., Ding, Y., et al., 2023b. Rapid and Effective Lead Elimination Using Cow Manure Derived Biochar: Balance between Inherent Phosphorus Release and Pollutants Immobilization. 11, 11010001. <https://doi.org/10.3390/toxics11010001>.
- Wu, J., Li, Z., Huang, D., et al., 2020. A novel calcium-based magnetic biochar is effective in stabilization of arsenic and cadmium co-contamination in aerobic soils. *Journal of Hazardous Materials*. 387, 122010 <https://doi.org/10.1016/j.jhazmat.2019.122010>.
- Xia, Y., Tang, Y., Shih, K., et al., 2020. Enhanced phosphorus availability and heavy metal removal by chlorination during sewage sludge pyrolysis. *Journal of Hazardous Materials*. 382, 121110 <https://doi.org/10.1016/j.jhazmat.2019.121110>.
- Xiao, J., Hu, R., Chen, G., et al., 2020. Facile synthesis of multifunctional bone biochar composites decorated with Fe/Mn oxide micro-nanoparticles: Physicochemical properties, heavy metal sorption behavior and mechanism. *Journal of Hazardous Materials*. 399, 123067 <https://doi.org/10.1016/j.jhazmat.2020.123067>.
- Xu, J., Hu, C., Wang, M., et al., 2022. Changeable effects of coexisting heavy metal on transfer of cadmium from soils to wheat grains. *Journal of Hazardous Materials*. 423, 127182 <https://doi.org/10.1016/j.jhazmat.2021.127182>.
- Xu, X., Schierz, A., Xu, N., et al., 2016. Comparison of the characteristics and mechanisms of Hg(II) sorption by biochars and activated carbon. *Journal of Colloid and Interface Science*. 463, 55–60. <https://doi.org/10.1016/j.jcis.2015.10.003>.
- Yan, C., Jin, J., Wang, J., et al., 2022. Metal-organic frameworks (MOFs) for the efficient removal of contaminants from water: Underlying mechanisms, recent advances, challenges, and future prospects. *Coordination Chemistry Reviews*. 468, 214595 <https://doi.org/10.1016/j.ccr.2022.214595>.
- Yang, F., He, Z., Yu, F., et al., 2023. Biomass inherent metal interfere carbothermal reduction modification of biochar for Cd immobilization. *Science of the Total Environment*. 867, 161425 <https://doi.org/10.1016/j.scitotenv.2023.161425>.
- Zhang, H., Shao, J., Zhang, S., et al., 2020a. Effect of phosphorus-modified biochars on immobilization of Cu(II), Cd(II), and As(V) in paddy soil. *Journal of Hazardous Materials*. 390, 121349 <https://doi.org/10.1016/j.jhazmat.2019.121349>.
- Zhang, H., Liao, W., Zhou, X., et al., 2022a. Coefficient of pyrolysis temperature and potassium phosphate impregnation on characteristics, stability, and adsorption mechanism of phosphorus-enriched biochar. *Bioresource Technology*. 344, 126273 <https://doi.org/10.1016/j.cej.2022.139809>.
- Zhang, Y., Liu, J., Zhang, F., 2020b. Risk assessment of nitrogen, phosphorus, organic carbon, and heavy metal in Shanghai aquaculture ponds. *Journal of Fishery Sciences of China*. 27, 1448–1463. <https://doi.org/10.3724/SP.J.1118.2020.20107>.
- Zhang, H., Tian, S., Zhu, Y., et al., 2022b. Insight into the adsorption isotherms and kinetics of Pb(II) on pellet biochar via in-situ non-destructive 3D visualization using micro-computed tomography. *Bioresource Technology*. 358, 127406 <https://doi.org/10.1016/j.biortech.2022.127406>.